Dynamics of a freely evolving, two-dimensional granular medium

Sean McNamara*
Groupe Matière Condensée et Matériaux (URA CNRS No. 804), Université de Rennes I, Campus de Beaulieu, 35042 Rennes Cedex, France

W. R. Young†
Scripps Institution of Oceanography, La Jolla, California 92093-0230
(Received 15 September 1995)

We consider the dynamics of an ensemble of identical, inelastic, hard disks in a doubly periodic domain. Because there is no external forcing the total energy of the system is monotonically decreasing so that this idealized granular medium is ''cooling down.'' There are three nondimensional control parameters: the coefficient of restitution r, the solid fraction ν, and the total number of disks in the domain N. Our goal is a comprehensive description of the phenomenology of granular cooling in the (r,ν,N) parameter space. Previous studies have shown that granular cooling results in the formation of structures: both the mass and the momentum spontaneously become nonuniform. Four different regimes (kinetic, shearing, clustered, and collapsed) have been identified. Starting with the almost elastic case, in which r is just less than 1, the kinetic regime resembles a classical nondissipative gas in which there are no structures. When r is decreased (with fixed N and ν) the system evolves into the shearing regime in which most of the energy and momentum resides in the gravest hydrodynamic shear mode. At still smaller values of r the clustered regime appears as an extended transient. Large clusters of disks form, collide, breakup, and reform. From the clustered state the gas eventually either evolves into the shearing regime or, alternatively, collapses. The collapsed regime is characterized by a dynamical singularity in which a group of particles collides infinitely often in a finite time. While each individual collision is binary, the space and time scales decrease geometrically with the cumulative number of collisions so that a multiparticle interaction occurs. The regime boundaries (i.e., the critical values of r) in the (N,ν) plane have been delineated using event-driven numerical simulations. Analytic considerations show that the results of the simulations can be condensed by supposing that the critical values of r depend only on N and ν through the optical depth, $\lambda \equiv d\sqrt{N\pi\nu}/2$ where d is the disk diameter. [S1063-651X(96)03505-2]

PACS number(s): 47.50.+d, 05.20.Dd, 47.55.Kf, 62.90.+k

I. INTRODUCTION

A granular medium is often idealized as an ensemble of particles in which the energy loss that accompanies the collision of macroscopic bodies is modeled with a coefficient of restitution. In this paper we are concerned with the simplest case in which the particles are identical, circular hard disks moving ballistically in a two-dimensional, doubly periodic domain. Our goal is the identification and quantification of the different regimes which occur when this idealized two-dimensional granular medium ''cools.'' By this we mean that the disks start at $t=0$ in a thermalized state and then the gas freely evolves without the addition of energy. There are no interparticle forces between collisions and if these collisions conserve energy then this is the classical hard core gas. But if the coefficient of restitution is less than one then the collisions dissipate energy and so the granular temperature will decrease. If the particles simply slowed down as a result of this dissipation then granular cooling would be boring. But several earlier works have shown that inelastic dynamics also results in the formation of large scale inhomogeneities of both mass and momentum. In other words, granular cooling is accompanied by structure formation and these effects are often so dramatic that it is not an exaggeration to describe them as ''phase changes.''

The granular cooling problem was formulated by Haff [1] and he showed that granular kinetic theory predicts that the temperature decreases as t^{-2}. This law assumes that large scale structures do not form in the medium so that collision frequencies can be estimated using the average particle separation. The t^{-2} prediction was tested by the one-dimensional simulations of McNamara and Young [2,3] and Sela and Goldhirsch [4] which showed that the cooling granular medium is unstable to the formation of clusters, i.e., the homogeneous state assumed by Haff is unstable. Once the structures form there are large departures from the t^{-2} law.

The two-dimensional cooling problem was investigated by Goldhirsch and Zanetti [5] and Goldhirsch, Tan, and Zanetti [6]. Using a combination of theory and numerical simulation these investigators showed that clustering occurs in a two-dimensional cooling medium. One interesting result, which has no one-dimensional precursor, is that in some cases the hydrodynamic shear modes are unstable so that a large scale segregation of momentum spontaneously appears.

Another phenomenon which occurs in cooling granular systems is inelastic collapse. Bernu and Mazighi [7], and later McNamara and Young [2] and Constantin, Grossman,

*Electronic address: sean@dpmsun1.univ-lyon1.fr
Present address: DPM, Physique des Materiaux, Université Claude Bernard Lyon I, 43 boulevard du 11 Novembre 1918, 69622 Villeurbanne Cedex, France.
†Electronic address: bill@dalek.ucsd.edu

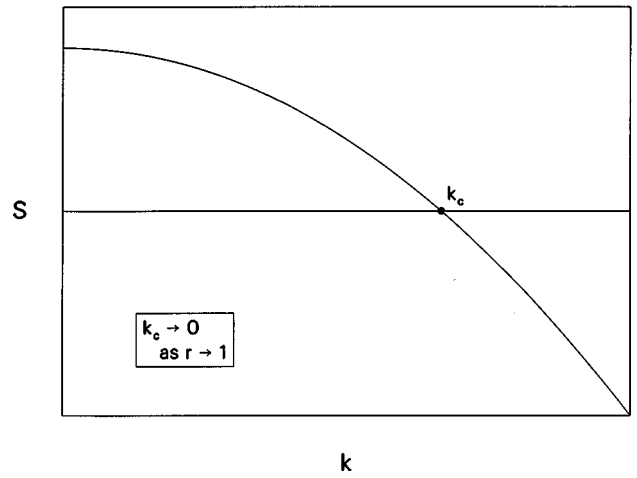

FIG. 1. A schematic linear stability curve showing the growth rate s as a function of the wave number k [i.e., linear disturbances are proportional to $\exp(s\tau+ikx)$ where τ is a ''collision time'' introduced in Refs. [3], [5], [6], and [19]]. Disturbances with wave numbers less than k_c are unstable, i.e., long waves are unstable. If the domain is sufficiently small then these long waves will be unable to satisfy the quantization condition and the homogeneous state will be stable.

and Mungan [8], showed that inelastic particles in one dimension have a collective behavior which results in a multiparticle collision. A group of inelastic particles can collide infinitely often in a finite time so that the interparticle spacing becomes zero and all of the kinetic energy in the center of mass frame is dissipated. This sequence of binary collisions, with geometrically decreasing space and time scales, accumulates in a true multiparticle collision. Thus the binary collision assumption, which is used in granular kinetic theories, fails. McNamara and Young [9] presented numerical evidence that this finite time singularity also occurs in two dimensions. One goal of this paper is to delineate the region of the parameter space in which the inelastic collapse occurs in a cooling, two-dimensional granular medium.

An important characteristic of the instabilities described above is that they are confined to long wavelengths, or small wave numbers. Consequently small systems will be stable because the long, unstable waves will not fit in the domain. If the particle density is fixed then this condition on the domain size is equivalent to saying that the clustering instability requires a certain minimum number of particles. As the coefficient of restitution r approaches one the band of unstable wave numbers contracts towards the origin as shown schematically in Fig. 1. Thus perfectly elastic systems are always ''small'' in the sense that as $r\to 1$ the unstable disturbances become arbitrarily long so that structures cannot form in a domain of fixed size.

The two-dimensional cooling problem in a doubly periodic geometry is complicated because there are three important nondimensional parameters. There is the coefficient of restitution r, the total number of disks N, and the solid fraction ν. If the square domain has a side of length L and the disk diameter is d then

$$\nu = N\,\frac{\pi d^2}{4L^2}. \tag{1}$$

Throughout this paper we use N, ν, and r as independent parameters and determine d/L from Eq. (1). Our goal here is a panoramic exploration of this three-dimensional parameter space. Thus our strategy differs from the earlier study of Goldhirsch, Tan, and Zanetti [6] which was based on simulations of dilute ($\nu=0.05$) and large ($N=20\,000$ or $N=40\,000$) systems with $r=0.6$ and $r=0.98$.

II. DESCRIPTION OF THE EVENT-DRIVEN SIMULATIONS

In this section we describe the model used in the simulations, the initial conditions, the boundary conditions, and how the smooth fields are estimated from the particle positions and velocities. We also explain the criterion used to detect inelastic collapse.

A. The collision rule

During a collision, the relative velocity of the particles perpendicular to the line connecting their centers is conserved, but the velocity along this line is reduced by a factor r. Thus the collision rule is

$$\begin{aligned} \mathbf{u}_1' &= \mathbf{u}_1 - \tfrac{1}{2}(1+r)[\hat{\mathbf{k}}\cdot(\mathbf{u}_1-\mathbf{u}_2)]\hat{\mathbf{k}}, \\ \mathbf{u}_2' &= \mathbf{u}_2 + \tfrac{1}{2}(1+r)[\hat{\mathbf{k}}\cdot(\mathbf{u}_1-\mathbf{u}_2)]\hat{\mathbf{k}}, \end{aligned} \tag{2}$$

where primes indicate velocities after the collision, and $\hat{\mathbf{k}}$ is a unit vector pointing along the line of centers, from particle 1 towards particle 2. Collisions are assumed to be instantaneous and involve only two particles. Between collisions particles move at a constant velocity.

B. Initial and boundary conditions

The initial condition for all simulations is a uniform distribution of particles in physical space and a Maxwellian distribution in velocity space. The initial condition is prepared by placing particles into the space on a regular array (to avoid interpenetrations) and assigning random velocities. The simulation is run with $r=1$, the value for an ideal gas, for at least 100 collisions per particle. This thermalization ensures that all trace of the initial array is erased and that the velocities are distributed with a Maxwellian velocity distribution. Then the resulting positions and velocities of the particles define the initial conditions for the inelastic simulations. Independent initial conditions can be generated by stopping the elastic simulation at different times.

We use a square domain with doubly periodic boundary conditions. When a particle leaves the right (or bottom) side of the domain, it reenters at the left (or top) with the same velocity. This simple boundary condition removes the need for specifying an interaction with walls.

C. The smoothing algorithm

The simulation gives the positions and velocities of each particle. But hydrodynamic theories describe continuous fields, usually the density ρ, macroscopic velocity v, and temperature T. To make the transition between a list of particle positions and smooth continuous fields we consider the mass of each particle to be spread out in a ''halo.'' (The

terminology is from an unpublished paper by Eckart [10].) The halo is larger than a particle diameter, meaning that halos of neighboring particles can overlap. To calculate ρ, v, or T at any point, the contributions from the nearby halos are summed. To make this idea precise, define the halo function $h(R)$ with the following properties:

$$\int_0^\infty h(R)2\pi R dR = 1,$$

$$h(R) \to 0 \quad \text{as} \quad R \to \infty, \tag{3}$$

$$h(R) \geqslant 0.$$

The halo function describes how the mass is distributed in the halo. The argument of h specifies the distance between the point in question and the center of the particle. The first condition in Eq. (3) is a normalization condition. The second property requires that the halo be localized around the particle's position. The third property guarantees that the density and temperature will be non-negative everywhere. We use a Gaussian halo function

$$h(R) = \frac{1}{2\pi\sigma^2} \exp(-R^2/2\sigma^2), \tag{4}$$

where $\sigma > d$ is a length that controls the size of the halo. We typically use $\sigma/d = 6$. The density, macroscopic velocity and temperature at any point $\mathbf{x}$ can be calculated by

$$\rho(\mathbf{x}) = m\sum_{i=1}^{N} h(|\mathbf{x}_i - \mathbf{x}|), \tag{5a}$$

$$\rho(\mathbf{x})v(\mathbf{x}) = m\sum_{i=1}^{N} \mathbf{u}_i h(|\mathbf{x}_i - \mathbf{x}|), \tag{5b}$$

$$\rho(\mathbf{x})T(\mathbf{x}) = m\sum_{i=1}^{N} (u_i^2/2)h(|\mathbf{x}_i - \mathbf{x}|) - \rho(\mathbf{x})v^2(\mathbf{x})/2, \tag{5c}$$

where N is the number of particles in the simulation, $\mathbf{x}_i$ is the location of the ith particle, and $\mathbf{u}_i$ is its velocity. The advantage of this smoothing technique is that these expressions are continuous in space and time and gradients can be calculated by differentiating Eq. (5).

D. The event driven strategy and the contact criterion for collapse detection

The simulation advances from one collision to the next. Particles participating in all impending collisions are identified, and the time of each collision is forecast. Then the colliding pair with the shortest time to collision is located, and the system is advanced to that time. The velocities of the two particles after collision are calculated using Eq. (2). Then the list of future collisions is updated, and the cycle begins again. This movement in time from one collision to another is called ''event driven'' [11,12]. In contrast, the ''soft-particle'' method requires small time steps. For a comparison between soft-particle, time stepped and the hard-particle, event-driven algorithms for granular systems, we refer the reader to the review by Haff [13] and also to the recent work of Luding *et al.* [14].

In an ideal gas, instantaneous collisions will always be binary, because a three body interaction requires that two collisions be simultaneous. However, in a granular medium, multiple particle collisions occur with a finite probability [9]. These interactions are as close to simultaneous as machine precision permits. Thus the ''hard-particle'' model, with its binary collision rule in Eq. (2), is not defined the first time a multiple-particle collision occurs. Model regularization requires additional rules which specify the outcome of a multiparticle collision, e.g., the largest relative velocity (LRV) procedure described by Luding *et al.* [15]. In this paper we will not become involved in the regularization issue: instead we use a ''contact criterion'' to detect three particle interactions.

To explain the ''contact criterion'' for collapse detection we begin by observing that after every binary collision, the future collisions of the two colliding particles must be recalculated. If any one of these future collisions involve a third particle separated by less than 10^{-15} of a particle diameter, then we stop the program. At this point the interparticle spacing (and hence the time to the next collision) cannot be calculated without incurring a large round off error. Thus when the program stops, there are two particles in contact, and a third particle within $10^{-15}d$ of one of the colliding pair. To within machine precision, a three-body interaction has occurred.

Figure 2 shows the contact criterion in action. Two simulations are superimposed. The first, indicated by circles, stops when a three-body event is detected, while the second, with the same initial conditions and indicated by crosses, continues to evolve after the three-body event. Each time the program calculates a particle separation, a point is placed on the graph, whether it leads to a collision or not. For the first 100 times that the program calculates a particle separation, it finds a separation greater than $10^{-2}d$. Then, a three-body interaction commences. The particle separation decreases geometrically over 14 orders of magnitude, until it hits the floor of machine precision at $10^{-15}d$. At this point, the contact criterion halts the first simulations, while the second continues. This second simulation generates four separations, all at the limit of machine precision (and two of which are negative), before the particles disperse. We believe that on a machine with infinite precision, the geometrically decreasing separations would continue forever. If the contact criterion is ignored, this infinite series of collisions is replaced by four or five inaccurately calculated collisions, after which the cluster disperses. We do not know what effects, if any, this ''numerical regularization'' has on other aspects of the simulations. It is possible that the effect is negligible, because neither the infinite series of collisions, nor the four or five collisions that take their place dissipate much energy.

Now, in the one-dimensional case, analytic results [2,7,8] show that true multiparticle collisions occur. But an analogous analytic framework has not yet been constructed for the two-dimensional case. In this paper whenever a simulation is stopped by the contact criterion we say that the simulation ''stopped because of an inelastic collapse.'' Evidence supporting this interpretation is given in Ref. [9]: the nearly three-body events are associated with a diverging collision count and a line of particles. In the sequel additional evi-

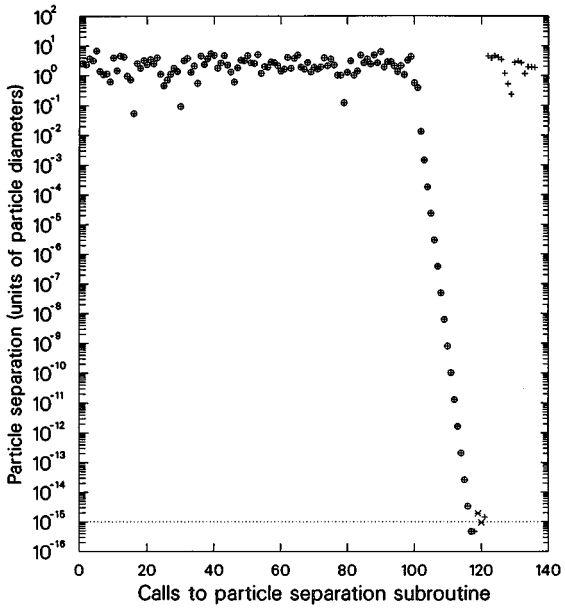

FIG. 2. The contact criterion in action. Two simulations are shown, one which respects the contact criterion (circles), and one which does not (crosses). The two simulations have the same initial conditions. Each time the program calculates a particle separation, a point is placed on the graph, whether it leads to a collision or not. After about 100 calls to the particle separation subroutine, inelastic collapse commences. The particle separations decrease geometrically, until hitting the floor of the machine precision. At this point, the first simulation is stopped by the contact criterion, whereas the second proceeds. We believe the following four separations, all at the level of numerical precision, are computational artifacts. Two of the separations (marked by stars) are negative. After these four collisions, the particles disperse.

dence is provided: two-dimensional three-body events occur only when r is below a certain critical value that is related to the analytically estimated threshold for a one-dimensional collapse.

III. PHENOMENOLOGY OF THE COOLING GRANULAR MEDIUM

In this section we present a set of simulations all with $N=1024$ particles and a solid fraction $\nu=0.25$. At this parameter setting the most important qualitative distinction is between simulations with small values of r which collapse, and those with larger values of r which seem to run indefinitely without encountering a multiparticle interaction. In Sec. IV we estimate that the critical value of r which separates these two regimes $r_{\rm crit}^{\rm coll}(1024,0.25)$, is around 0.62. We will describe this transition in more detail below. For the moment we will focus on moderately elastic simulations with $0.56\leqslant r\leqslant 1$.

For noncollapsing simulations, such as those described by Goldhirsch, Tan, and Zanetti [6], the major qualitative distinction is between cases in which mass and momentum are organized into large structures, and those in which mass and momentum remain smoothly distributed throughout the domain. Once again, this qualitative distinction is controlled by r. Very elastic simulations, i.e., at $(N,\nu)=(1024,0.25)$ those with $0.98\leqslant r\leqslant 1$, do not form organized structures.

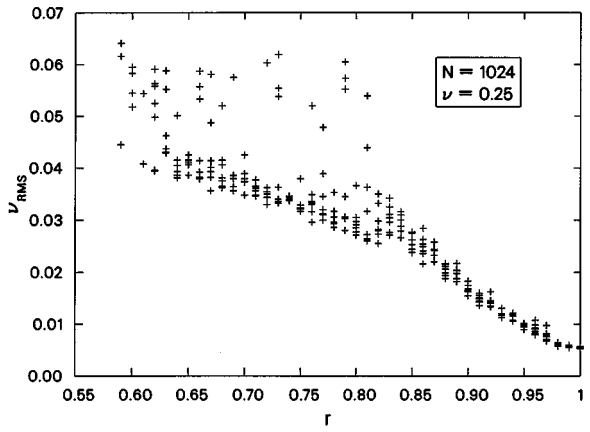

FIG. 3. Density in inhomogeneities measured by $\nu_{\rm rms}$, the root mean square (rms) fluctuation of the solid fraction, for 45 simulations with $0.55<r\leqslant 1.0$. Each simulation ran until either $C/N=800$, or until inelastic collapse. The time series of $\nu_{\rm rms}$ was divided into eight segments each of length $\Delta C/N=100$. The first segment of each time series was discarded, and the remaining seven averaged to generate points for this plot. If inelastic collapse occurred within a segment, that segment was also discarded.

Figures 3 and 4 show the results of 45 simulations with $0.56\leqslant r\leqslant 1$ and $\Delta r=0.01$. Each simulation ran until either the number of collisions per particle, denoted C/N, reached 800, or until the simulation was halted by collapse (this happened to the six simulations in the range $0.56<r<0.61$ and also to the simulation with $r=0.64$). Two quantities, $\nu_{\rm rms}$ and E_K/E_T (defined below), were recorded every $\Delta C/N=1$ collisions. Then this record was divided into eight segments of $\Delta C/N=100$, and collision weighted (*not* time weighted) average values of these quantities were computed within each segment. The first segment was dropped, because it contains transients. We also discarded segments in which a collapse occurred. The remaining segments make up the data of Figs. 3 and 4. Notice that there are no points for $r\leqslant 0.58$: this is because in these three simulations collapse occurred in the first segment. On the other hand when $r\geqslant 0.62$ there are

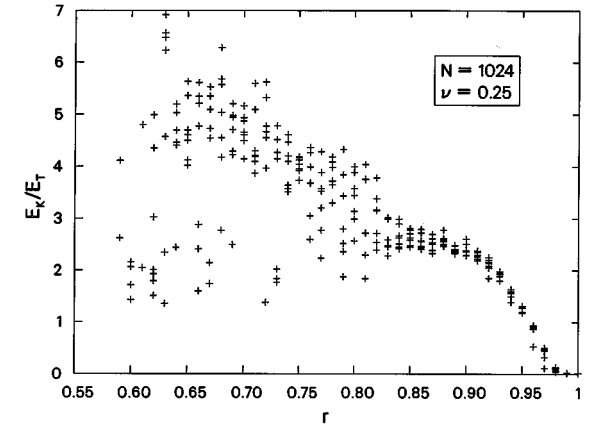

FIG. 4. This figure shows the same 45 simulations as Fig. 3, except that the momentum inhomogeneities, measured by the ratio of macroscopic kinetic to thermal kinetic energy E_K/E_T, are shown.

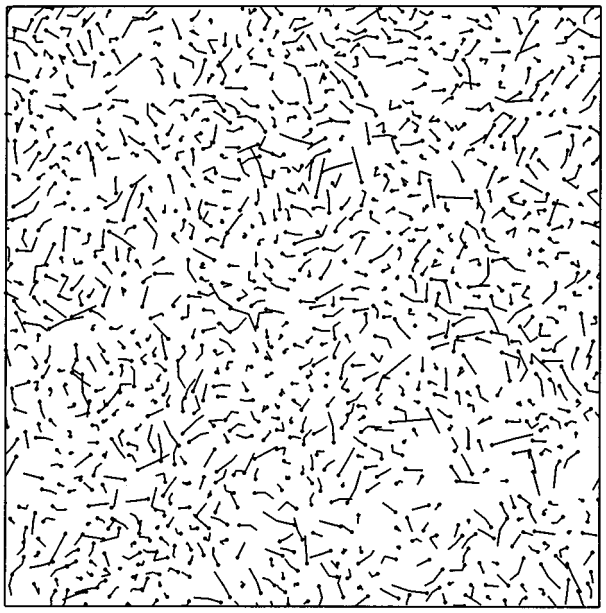

FIG. 5. Particle streaklines in the kinetic state. Here, $r=0.98$, $N=1024$, and $\nu=0.25$. $C/N=600$ collisions have occurred since the simulation began. The dot marks the initial position of each particle, and the line tracks the particle position for a small amount of time. Even though $E_K/E_T=0.98$, which is much greater than the average value $E_K/E_T=0.016$ for $r=1.0$, we classify this simulation as ''kinetic,'' because there is no sign of the large scale velocity organization which is visible in Fig. 7.

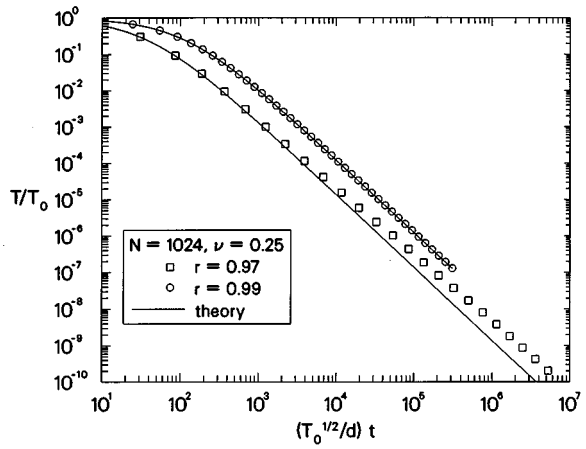

FIG. 6. The ''granular temperature'' vs time for simulations at $r=0.99$ and $r=0.97$ (all with $N=1024$, $\nu_0=0.25$). The circles and squares show results from simulations, and the continuous curves are predictions from the kinetic theory in Eq. (7). The temperature is nondimensionalized with T_0, the temperature at $t=0$, and the time with $d/T_0^{1/2}$, the average time for a particle to travel its diameter when $T=T_0$.

seven data points at almost every value of r. The exception is $r=0.64$ which collapsed when the number of collisions per particle was $C/N=774$.

In Fig. 3, density organization is measured by $\nu_{\rm rms}$, the root mean square (rms) variation of the local solid fraction $\nu(\mathbf{x})$. The local solid fraction is evaluated on a grid of points, using the method described in Sec. II C. Then $\nu_{\rm rms}$ is calculated as the square root of the area average of $[\nu(\mathbf{x})-\nu]^2$.

In Fig. 4 momentum organization is measured by the ratio of macroscopic to thermal kinetic energy. The temperature and the macroscopic velocity were calculated on a grid of points, again using the smoothing algorithm of Sec. II C. Then the quantity E_K/E_T is the ratio of the total macroscopic kinetic energy, $E_K=\int\rho\mathbf{v}\cdot\mathbf{v}/2dA$, to the total thermal energy, $E_T=\int\rho TdA$, where $\mathbf{v}$ and T are defined in (5b) and (5c). The ratio E_K/E_T is also effectively a squared Mach number.

These two diagrams give one a rough idea of how the momentum and mass organization depends on r and we now discuss the different regimes in turn.

A. The kinetic state: $0.98\leqslant r\leqslant 1.0$

The first region $0.98\leqslant r\leqslant 1$ is characterized by low values of both $\nu_{\rm rms}$ and E_K/E_T, indicating that the density and particle velocities are not well organized. A ''streakline'' visualization of the simulation with $r=0.98$ (Fig. 5) confirms that there are no obvious mass or momentum correlations. This is not surprising because this part of parameter space contains the ideal gas at $r=1$, whose equilibrium is this ''kinetic'' state. The kinetic state also exists for r slightly less than 1, with the particles remaining evenly distributed with uncorrelated velocities, but the average velocity dropping slowly as energy is dissipated by the slightly inelastic collisions. The stability of this gaseous state when $r<1$ requires that the domain be small so that the unstable long wave disturbances are excluded—see Fig. 1 and the surrounding discussion.

In the kinetic state the granular kinetic theories make accurate predictions. The two-dimensional theory of Jenkins and Richman [16,17] can be used to calculate the loss of granular thermal energy through collisions. Equations describing the kinetic state can be found by assuming that $\mathbf{v}=0$ and that the density ρ, and the temperature, T, are constant in space. Then the temperature equation reduces to

$$\frac{\partial T}{\partial t}=-\gamma T=-\frac{8}{\sqrt{\pi}}(1-r)\frac{\nu}{s_*(\nu)d}T^{3/2}, \tag{6}$$

where we have used the notation of Ref. [18]: d is the particle diameter, $s_*(\nu)\equiv(1-\nu)^2/(1-7\nu/16)$, and T and t are the dimensional temperature and time, respectively. The solution of Eq. (6) is

$$T=T_0\left[1+\frac{4}{\sqrt{\pi}}(1-r)\frac{\nu T_0^{1/2}}{s_*(\nu)d}t\right]^{-2}, \tag{7}$$

where T_0 is the temperature at $t=0$. When t is large, $T\propto t^{-2}$. Equation (7) is compared with simulations in Fig. 6. The theoretical prediction has a maximum error of 1.5% in the $r=0.99$ simulation. Simulations at $r=0.98$ (not shown) have a much larger error (15%). However, the temperature drops several orders of magnitude during these simulations, so the kinetic theory still provides an impressive prediction. The $r=0.97$ simulation deviates from the t^{-2} prediction. This simulation is in the ''shearing state.''

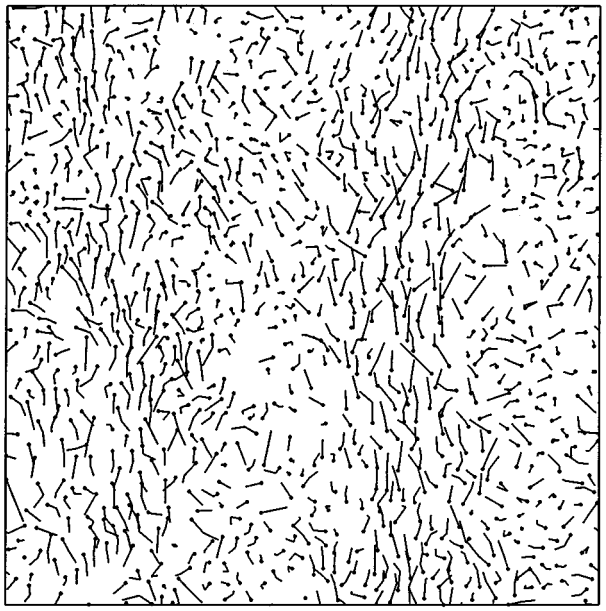

FIG. 7. Particle streaklines for the shearing state. Here, $r=0.97$, $N=1024$, and $\nu=0.25$. $C/N=400$ collisions have occurred since the simulation began. The dot marks the initial position of each particle, and the line tracks the particle position for a small amount of time. The momentum is organized into the gravest shear mode.

B. The shearing state: $0.83 \leqslant r \leqslant 0.97$

In the second region, $0.83 \leqslant r \leqslant 0.97$, $\nu_{\rm rms}$ in Fig. 3 increases smoothly as r decreases. E_K/E_T in Fig. 4 increases to the plateau value of about 2.5. These simulations are in the ''shearing'' state described by Goldhirsch and Zanetti [5]. As shown in Fig. 7, the particles are divided into two bands which move in opposite directions. This global motion contains a large fraction of the total kinetic energy and this leads to high values of E_K/E_T in Fig. 4. Figure 7 is not typical of the shearing state because $r=0.97$ is just beneath the shearing–kinetic boundary. For values of r well away from the regime boundaries the concentration of momentum into the large-scale shear flow is much greater, and also the mass is clearly concentrated into the centers of the two counterflowing streams [5,6].

C. The clustering state: $0.59 \leqslant r \leqslant 0.82$

Around $r=0.82$, the data in Figs. 3 and 4 split into two populations. In Fig. 8, we plot E_K/E_T vs $\nu_{\rm rms}$ for simulations in Figs. 3 and 4 with $0.55 \leqslant r \leqslant 0.82$. This regression reveals that there are two distinct populations: one with $3<E_K/E_T<7$ and $0.025<\nu_{\rm rms}<0.04$, and another population with $1<E_K/E_T<3$ and $0.04<\nu_{\rm rms}<0.065$. A closer inspection of these two groups shows that the high E_K/E_T points are in the shearing state described above in Sec. III B but the second group, with the smaller ratio E_K/E_T, is in a ''clustering'' state. In the clustered state the particles are gathered into bunches which collide, breakup, and then reform. This clustering has been seen previously in a simulation with $\nu=0.05$, $r=0.6$, and $N=40{,}000$ by Goldhirsch, Tan, and Zanetti [6].

Figure 8 shows that the clustered state is an ''extended transient.'' The +'s, which indicate the quantities averaged between $C/N=20$ and $C/N=100$, all lie near the clustered state, whereas the $\times$'s, which indicate the values averaged between $C/N=700$ and $C/N=800$, all lie in the shearing state. All our clustering simulations eventually either made a transition to the shearing state or collapsed. We have never seen a simulation in the shearing state return to the clustering state.

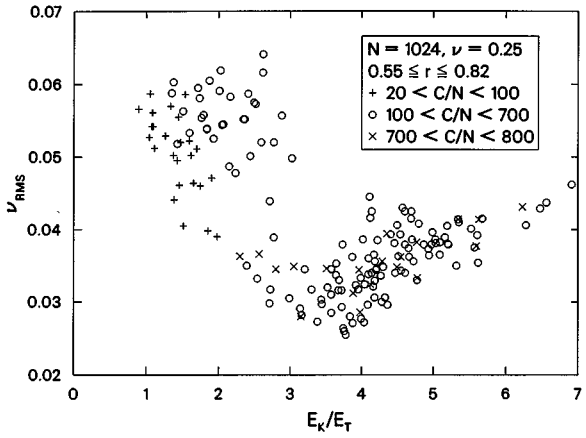

FIG. 8. The correlation between $\nu_{\rm rms}$ and E_K/E_T for the simulations in Figs. 3 and 4 with $0.55 \leqslant r \leqslant 0.82$. This regression shows two populations. The crosses indicate the average of all simulations between $C/N=20$ and $C/N=100$; these points are *not* shown in Figs. 3 and 4. The $\times$'s mark the averages between $C/N=700$ and $C/N=800$. We conclude that the simulations begin in the high $\nu_{\rm rms}$ moderate E_K/E_T population (the clustering state), and finish in the moderate $\nu_{\rm rms}$, high E_K/E_T state (shearing state).

Figure 9 shows a time series of E_K/E_T, $\nu_{\rm rms}$ and a measure of the velocity anisotropy for the simulation with $r=0.73$. The transition from the clustering state to the shearing state at $C/N \approx 400$ is obvious in all three of these quantities. Figure 10 shows two particle ''streakline'' snapshots for this particular simulation. In Fig. 10(a), $C/N=100$ and the system is in the clustering state. In Fig. 10(b), $C/N=800$ and the organized, large scale flow which is characteristic of the shearing state is evident.

We summarize these results with $N=1024$ and $\nu=0.25$ by saying that simulations with $0.59<r \leqslant 0.82$ follow a different evolutionary route than those with $0.83 \leqslant r \leqslant 0.97$. When $0.59 \leqslant r \leqslant 0.82$, clusters form initially, but subsequently the system either collapses or evolves into the shearing state, and then remains there. When $0.83 \leqslant r \leqslant 0.97$ the system evolves directly into the shearing state without a clustering sojourn.

D. Inelastic collapse

Below a certain value of r, the evolution of the simulations is stopped by an inelastic collapse [9]. When r is close to 0, only a few particles are required for collapse, and collapse occurs quickly when there are many particles in the domain. For example, in Fig. 11, we show the final state of a $N=1024$, $\nu=0.25$, $r=0.05$ simulation. The simulation has stopped after only 31 collisions, and the particles involved in these collisions are shaded black. The majority of particles have not suffered a single collision, and retain their initial kinetic energy. All black particles in Fig. 14 appear in pairs,

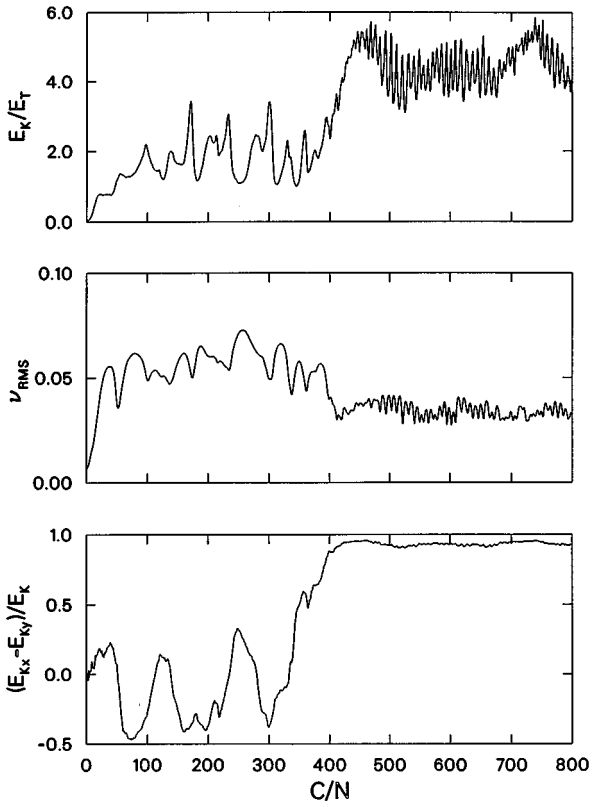

FIG. 9. Time series for a simulation with $N=1024$, $\nu=0.25$, and $r=0.73$. Top panel: The momentum organization E_K/E_T. Middle panel: The density organization $\nu_{\rm rms}$. Bottom panel: The velocity anisotropy: $\Sigma(u_i^2-v_i^2)/(u_i^2+v_i^2)$ where (u_i,v_i) is the velocity of particle i. In all three panels the transition from the clustered to the shearing state at $C/N\approx 400$ is clear.

except for the line of three particles in the lower right corner. These three are the particles causing the collapse and they are responsible for 14 of the 31 collisions that have occurred in this simulation. (The three particles do not have to be perfectly aligned. At $r=0.05$, numerical simulations show that if the velocities *are* perfectly aligned, and the particle surfaces are initially separated by a particle diameter, collapse will occur if either of the two particles that collide first deviate no more than about 0.03 of a particle diameter from a straight line. On the other hand, the third particle can deviate by as much as a 1/8 of a particle diameter. At $N=1024$, $\nu_0=0.25$, and $r=0.05$, these arrangements are common enough in the initial condition to always halt the simulation before every particle has had a chance to participate in a collision.)

The linear arrangement of the three disks in Fig. 11 indicates that an inelastic collapse is a one-dimensional phenomenon. In Sec. IV we argue that once a sufficient number of particles (given by the one-dimensional theory) are lined up, then collapse occurs just as it does in one dimension. In support of this conclusion we show in Fig. 12 a selection of simulations all with $N=1024$ and $\nu=0.25$ that were stopped by collapse. The disks that were involved in the most recent 200 collisions are shaded black. The shading reveals the roughly linear structures that form near the time of collapse.

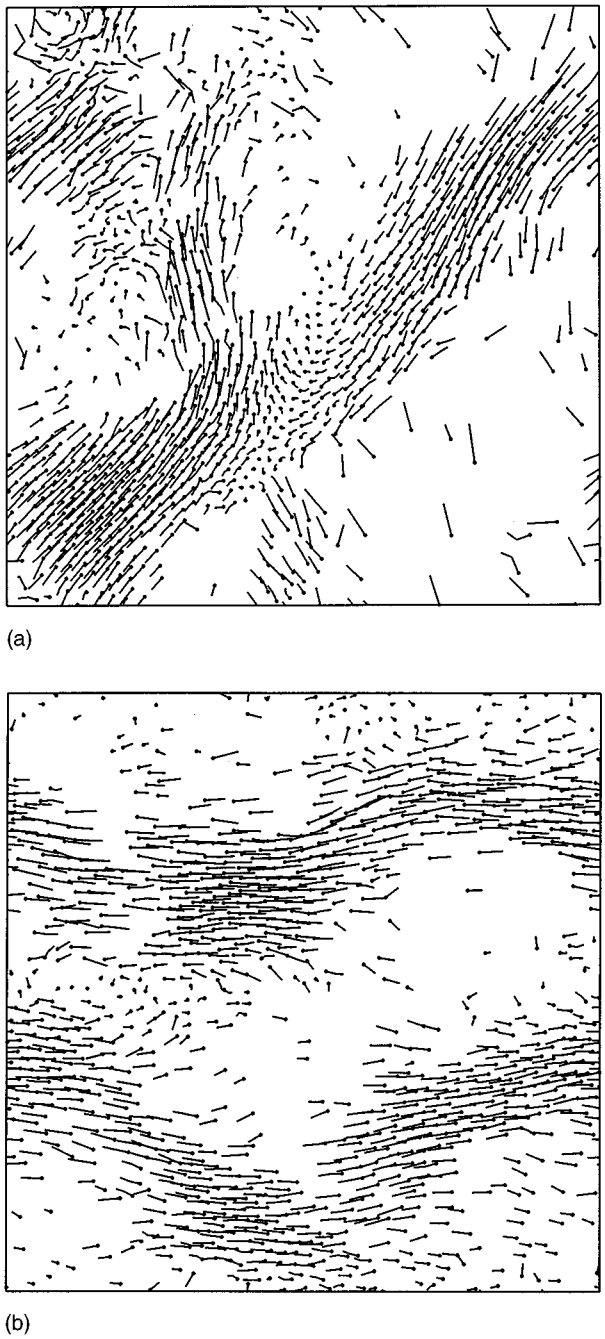

FIG. 10. (a) Particle streaklines for the clustering state. Here, $r=0.73$, $N=1024$, and $\nu=0.25$. $C/N=100$ collisions have occurred since the simulation began. The dot marks the initial position of each particle, and the line tracks the particle position for a small amount of time. (b) The same simulation as (a), but at a later time $C/N=800$. The system is now in the shearing state.

IV. REGIME BOUNDARIES

In this section, we will compare the predictions of kinetic theories to our simulations. One issue here is how well these theories predict the boundary between the kinetic and shearing states. We express these boundaries as critical values of r where the transition occurs for fixed values of N and ν. For example, with $N=1024$ and $\nu=0.25$ (Figs. 3 and 4), the boundary between the shearing and kinetic states is

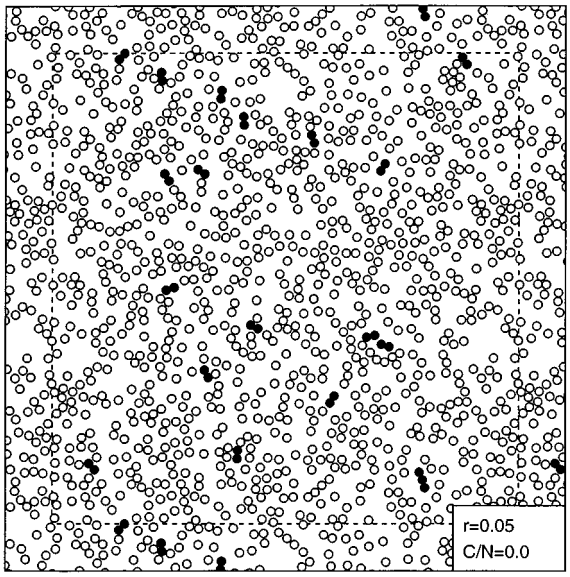

FIG. 11. A simulation at $N=1024$, $\nu_0=0.25$, and $r=0.05$ which stops after just 31 collisions due to inelastic collapse. All particles involved in any collision are colored black. The line of the three particles in the lower right hand corner is the collapsing triad. These three particles account for 14 of the 31 collisions.

$r_{\rm crit}^{\rm SK}(1024,0.25)\approx 0.97$ and the critical value for collapse is $r_{\rm crit}^{\rm coll}(1024,0.25)\approx 0.62$.

One of our main conclusions is that the strong dependence of these critical values on N and ν can be expressed in terms of a single parameter viz., the ''optical depth'' λ. This length is defined by

$$\lambda \equiv \nu L = \left(\frac{d}{2}\right)\sqrt{N\pi\nu}, \tag{8}$$

where L is the domain size in Eq. (1). The optical depth has a simple physical meaning. If one imagines a ray of light passing directly across the simulation, from one boundary to the other, then the ray travels a distance L. Now, the fraction of the area covered by disks is ν, so νL is the distance the ray travels *inside* particles, hence the term ''optical depth.'' Alternatively, if all the particles were compressed against one boundary, they would form a layer approximately $\lambda=\nu L$ thick.

The dependence of both $r_{\rm crit}^{\rm SK}$ and $r_{\rm crit}^{\rm coll}$ on the combination of N and ν in λ hints that the processes which characterize the different regimes are essentially one dimensional because the optical depth gives the number of particles in a one-dimensional slice through the domain. The one dimensionality of the regime-changing mechanisms will be emphasized in the discussion below.

A. Determination of the critical coefficient of restitution for collapse

Precisely determining the threshold value $r_{\rm crit}^{\rm coll}(N,\nu)$ for which collapse occurs involves two ambiguities. First, the boundary moves as the number of collisions in the simulation increase. For example, for $N=1024$ and $\nu=0.25$, the collapse threshold is estimated to be $r=0.62$ if the simulations are run until $C/N=1500$, but $r=0.59$ if the simulations are run only to $C/N=400$. For larger values of N, or for larger solid fractions (e.g., $\nu=0.8$), the typical change is $\Delta r=0.05$. It is difficult to run all simulations to the same value of C/N, because simulations with small numbers of particles evolve much more quickly than large simulations. Therefore we adopted the arbitrary, but objective, procedure of running simulations until either collapse or until the total kinetic energy was reduced to 10^{-15} of the initial energy.

The second ambiguity is that the transition to collapse is not sharp, or at least with finite computer resources one can never compute long enough to be absolutely sure that a simulation will not collapse. In fact, there are large fluctuations when r is close to $r_{\rm crit}^{\rm coll}(N,\nu)$. Near this transition some simulations stop quickly because of collapse while others with identical values of (N,ν,r) run for a long time. To locate the transition in a consistent and meaningful way, we chose a set of values for r straddling the collapse threshold, and performed ten simulations at each value of r. Then we estimated the value of r where half the simulations collapsed. If two neighboring values of r collapsed with probabilities straddling 0.5, we linearly interpolated between these two points. If the probability of collapse was estimated to be 0.5 at more than one point, (this happened occasionally when there were local maxima or minima), we took the average. We carried out this procedure at many points in the (N,ν) parameter plane. Typically, the smallest value of r that never collapsed was about $\Delta r\approx 0.06$ greater than the largest value of r which always collapsed. Thus the uncertainty in our estimate of $r_{\rm crit}^{\rm coll}(N,\nu)$ is $\Delta r=\pm 0.03$.

The results of this survey are summarized in Fig. 13. For a fixed ν, increasing N increases $r_{\rm crit}^{\rm coll}(N,\nu)$, but each value of ν has its own curve. But if we plot $r_{\rm crit}^{\rm coll}(N,\nu)$ against λ/d as defined in Eq. (8), instead of N, then the data condense considerably—see Fig. 14.

It is interesting to compare the results of our *two-dimensional* simulations in Fig. 14 to the analytic estimates of $r_{\rm crit}^{\rm coll}$ of which have been obtained in the *one-dimensional* case. Bernu and Mazighi [7] using an ''independent collision wave model'' predict that

$$r_{\rm ICW}(N)=\tan^2\left[\frac{\pi}{4}\left(1-\frac{2}{N}\right)\right] \tag{9}$$

is the critical value of r for which N particles can collapse in one dimension. [Note that to obtain Eq. (9) we have taken Eq. (13) of Bernu and Mazighi and replaced their n by $N/2$. This is because Bernu and Mazighi are considering n particles colliding with a wall which is equivalent to a collision involving $N=2n$ particles in the middle of the medium.]

The second analytic estimate based on one-dimensional considerations is the ''cushion model'' (CM) of McNamara and Young [2]. This model expresses the number of particles required for collapse as a function of r, rather than the reverse. The result is

$$N_{\rm CM}(r)=\frac{\ln[(1-r)/4]}{\ln[(1+r)/2]}. \tag{10}$$

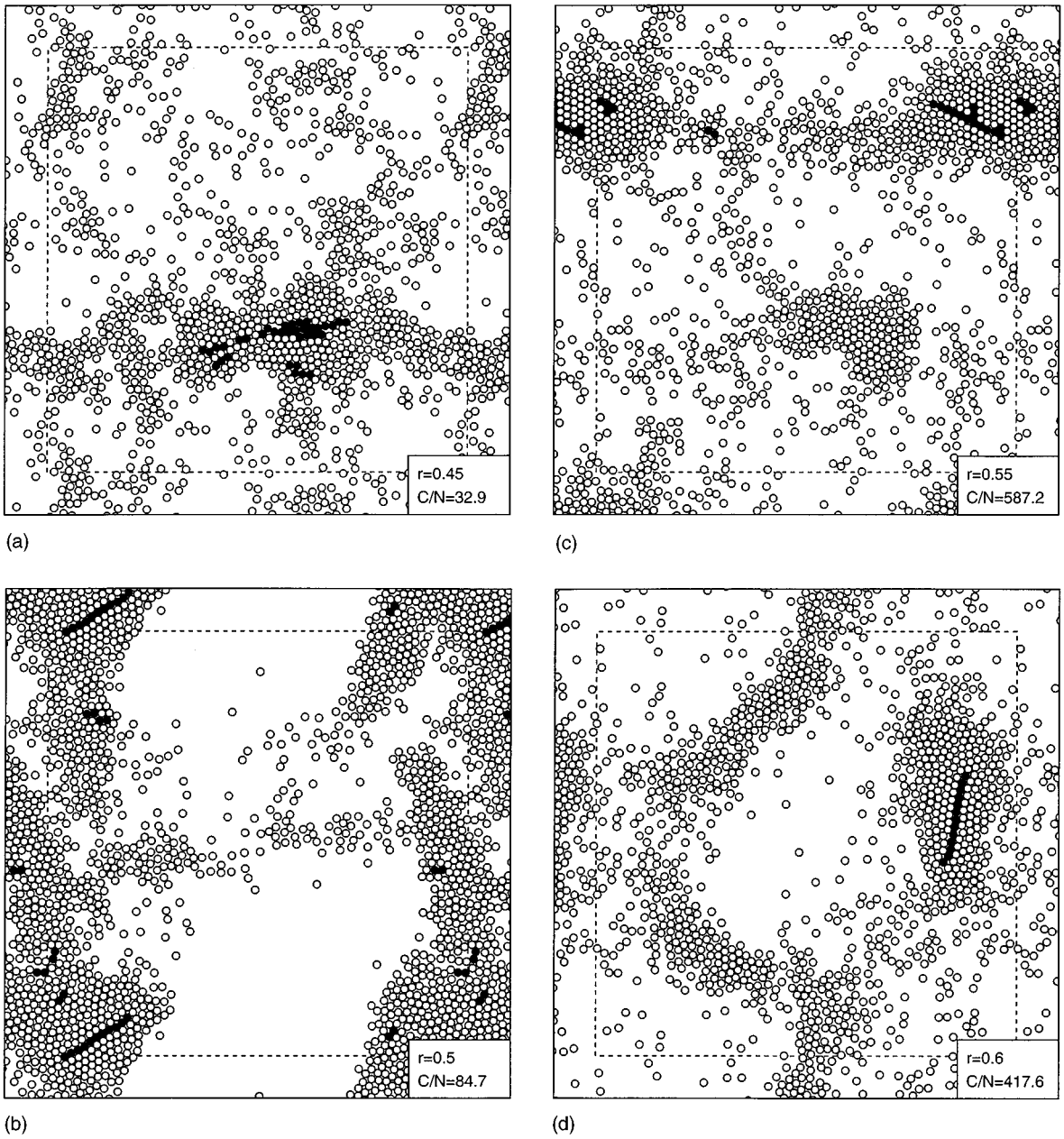

FIG. 12. This sequence of figures shows the final state of four simulations with $N=1024$, $\nu_0=0.25$, and the various values of r indicated in the bottom right hand corner of the figure. In all four cases the simulation was stopped by the collapse criterion: C/N is the total number of collisions per particle at the time the simulation is stopped. The particles involved in the last two hundred collisions are shaded black: the linear arrangements characteristic of collapse are evident.

After allowing for the factor of 2 which arises because we are considering conditions in the middle of a granular medium the expression in Eq. (10) is equivalent to Eq. (7) in McNamara and Young [2].

The two curves in Fig. 14 are obtained by replacing N in Eqs. (9) and (10) by $\lambda/d=\sqrt{\pi N\nu}/2$ and plotting the results in the (λ,r) plane. The proximity of the data points to these curves supports the suggestion from Figs. 11 and 12 that the collapse in two dimensions is essentially a one-dimensional process.

Although considering the position of the clustered-collapsed boundary as a function of the optical depth alone condenses the data, there is still a systematic variation in Fig. 14. At high optical depths, the curves for $\nu=0.25$ and $\nu=0.5$ are distinctly separated, although both parallel the one-dimensional collapse thresholds. At low optical depths, the data from different values of ν converge well, but diverge from the one-dimensional collapse threshold.

B. Kinetic-shearing boundary

In Sec. III B, we showed that when $N=1024$ and $\nu=0.25$, the kinetic state is unstable to the lowest shear mode if $r\leqslant 0.97$. This instability has been analyzed by two theoretical calculations. Goldhirsch, Tan, and Zanetti [5,6] explained the appearance of the shearing mode in their simulations by examining the linear stability of the dilute ($\nu\ll 1$), homogeneous, cooling granular medium. McNamara [19] analyzed

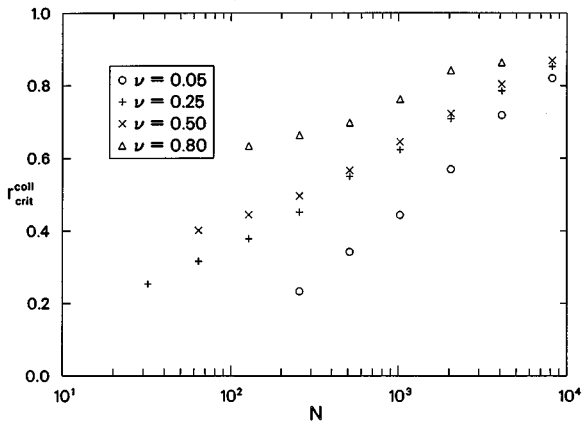

FIG. 13. The critical r for the inelastic collapse in the (r,N) plane for various values of ν. Note that points for different values of ν fall on separate curves.

the same problem with no restriction on ν. Both linear stability calculations relied on the granular kinetic theories of Jenkins and Richman [16,17,19].

The instability of the shearing modes is caused by a competition between the dissipation of thermal energy by the inelastic collisions and the rate at which viscosity transfers macroscopic kinetic energy to thermal energy. If viscosity damps shear waves more rapidly than the random thermal motions are dissipated in collisions, the system remains in the kinetic state. For instance, if one deliberately seeds the initial condition with a short wavelength shear wave then viscosity will quickly transfer the macroscopic kinetic energy of this short wave into thermal energy so that the system returns to the kinetic state.

But if the transfer of macroscopic kinetic energy from shear waves to thermal motion is less rapid than the inelastic dissipation of thermal energy then the kinetic energy in the shear waves ultimately dominates the flow. Goldhirsch and Zanetti [5] showed that this is what happens when the system enters the shearing state. For instance, consider the transition between $r=0.98$ (Fig. 5) and $r=0.97$ (Fig. 7). These two

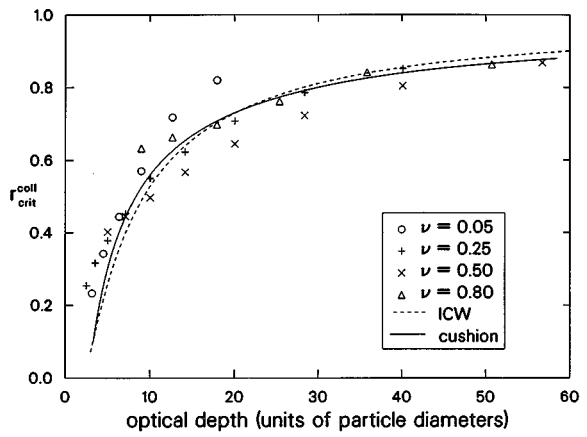

FIG. 14. The same data as Fig. 13, except the optical depth $\lambda \equiv \nu L$ is used as the abscissa. The separate lines from Fig. 13 have condensed.

simulations are distinguished by their organization of momentum ($E_K/E_T=0.098$ in Fig. 5 vs $E_K/E_T=0.484$ in Fig. 7, a factor of almost 5), rather than their organization of mass ($\nu_{\rm rms}=0.0064$ in Fig. 5 vs $\nu_{\rm rms}=0.0081$ in Fig. 7). We note that a similar transition has been observed in a related computational system [20].

Now, given r and ν, it is always possible to find a shear wave which is unstable in the sense described above, provided that the domain is large enough. The thermal energy lost by the collisions is independent of wavelength, but viscous damping of the shear modes decreases to zero as the wavelength becomes infinite. However the length of the shear waves that can exist in the simulation is limited by the finite size of the domain. In Fig. 7 ($r=0.97$), the flow is dominated by the longest wavelength shear mode that can fit in the simulation. In Fig. 5 ($r=0.98$), the shortest unstable wave is *longer* than the periodic domain, and so all possible shear waves are damped more rapidly than the medium cools. If the number of particles in that simulation were doubled with ν fixed at 0.25, then longer shear waves could fit in the domain, including one which is unstable.

We now summarize kinetic theory's quantitative prediction for the onset of the shearing instability and compare this prediction to our simulations. We use the results of Ref. [19] because they are not limited to the dilute case. Equation (21) in Ref. [19] gives the high wave number cutoff for the unstable shear modes as

$$\frac{k_c d}{\nu}=(1-r)^{1/2}\left(\frac{4}{\widetilde{\mu}_0(\nu)\sqrt{\pi}}\right)^{1/2}, \tag{11}$$

where k_c is the cutoff wave number of the instability (e.g., see Fig. 1), d is the diameter of the particles, and $\widetilde{\mu}_0(\nu) \equiv \nu^2\sqrt{\pi}+(\sqrt{\pi}/8)[\nu+s_*(\nu)]^2$ is a weak function of ν. The quantity $s_*(\nu)\equiv(1-\nu)^2/(1-7\nu/16)$ has appeared previously in Eq. (6).

We now use Eq. (11) to estimate the critical domain size by equating the wavelength of the shortest unstable shear mode $2\pi/k_c$ to L in Eq. (1). The resulting condition can be rearranged as

$$(1-r_{\rm crit}^{\rm SK})^{-1/2}=\frac{1}{2\pi}\left(\frac{4}{\widetilde{\mu}_0(\nu)\sqrt{\pi}}\right)^{1/2}(\lambda/d), \tag{12}$$

where λ is the optical depth defined in Eq. (8) and $r_{\rm crit}^{\rm SK}(\nu,N)$ is the critical value of the coefficient of restitution for the onset of the shearing instability if one operates with ν and N fixed.

Plotting $(1-r_{\rm crit}^{\rm SK})^{-1/2}$ against λ/d at the kinetic-shearing regime boundary for a fixed value of ν should yield a straight line passing through the origin with a slope given by Eq. (12). The slope of the line is a mild function of ν; therefore, results from several different ν should fall on separate, neighboring lines.

The critical value of the coefficient of restitution, i.e., $r_{\rm crit}^{\rm SK}$, was estimated from graphs like the one shown in Fig. 15. Many simulations with $N=1024$, $\nu=0.25$ were run at closely spaced values of r near the kinetic-shearing boundary. The final energy plotted in Fig. 15 is a sensitive measure of the energy dissipation, because every simulation runs for

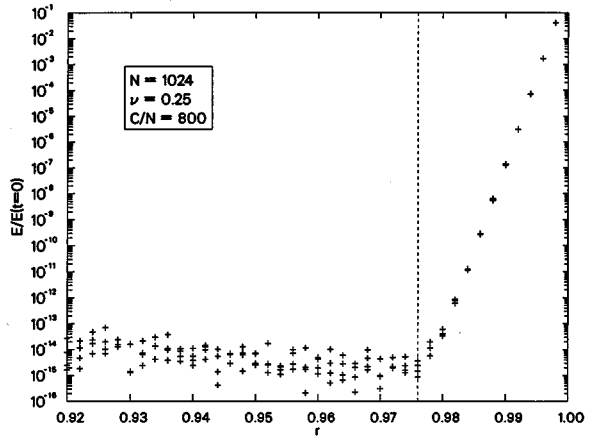

FIG. 15. Energy at $C/N=800$, normalized by the initial energy $E(t=0)$, for simulations at finely spaced values of r near the kinetic-shearing boundary. The vertical dotted line marks the boundary between shearing and kinetic regimes: this critical value is denoted by $r_{\rm crit}^{\rm SK}$. In the kinetic regime, the final energy depends strongly on r, but is nearly independent of r in the shearing regime. Plots like these were constructed for many values of N and ν, yielding the data in Figs. 16 and 17.

the same number of collisions: $C/N=800$. In the kinetic regime $r>0.976$ the final energy depends strongly on r because the majority of the energy is thermal energy which is dissipated directly in collisions at a rate depending strongly on r. In the shearing state, $r<0.976$, the majority of the energy resides in the longest shear wave. In order for this energy to be dissipated, it first must be converted into thermal energy by viscosity. Thus, the rate of dissipation is controlled by the viscosity, which is independent of r, so the final energy does not depend strongly on r.

Estimates of the kinetic-shearing boundary as a function of optical depth are shown in Fig. 16. For comparison with Eq. (12) we use $(1-r)^{-1/2}$ as the ordinate in Fig. 16. With the exception of $\nu=0.8$, the points fall on straight lines passing through the origin, consistent with Eq. (12). In Fig.

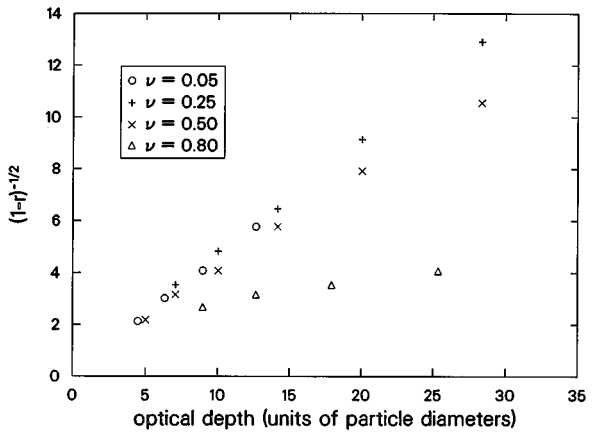

FIG. 16. This figure shows $(1-r_{\rm crit}^{\rm SK})^{-1/2}$ plotted against the optical depth λ/d. The different symbols distinguish different values of ν. Notice that the points belonging to a single value of ν fall on a straight line.

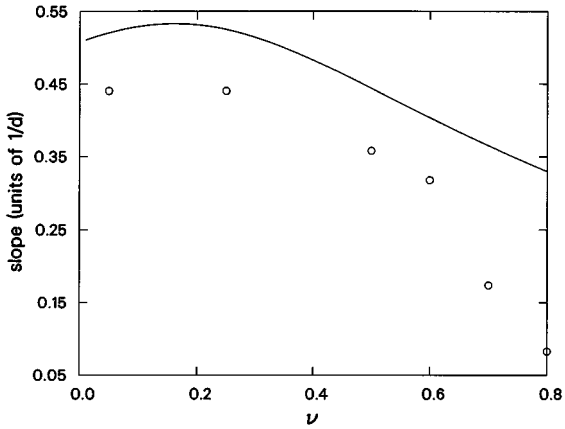

FIG. 17. The slopes of the lines in Fig. 16 for the four values of the solid fraction and two additional values (open circles). The solid line is the theoretical prediction of Eq. (10). All slopes are given in units of $1/d$, where d is the particle diameter.

17, we plot the slopes of the lines in Fig. 16 (open circles) against the theoretically predicted values from Eq. (12). In addition, two extra points, at $\nu=0.6$ and $\nu=0.7$ are added. The points with $\nu\leqslant 0.6$ parallel the theoretical curve, but deviate from it by a tantalizingly constant amount. We have no explanation for this offset. For $\nu=0.7$ and $\nu=0.8$ the points from our simulations depart strongly from the theoretical curve.

The failure of the theoretical prediction Eq. (12) for the dense simulations at $\nu=0.7$ and $\nu=0.8$ in Fig. 17 is probably related to the transition described by Jenkins and Shahinpoor [21]. This work predicted that a gas of hard disks ''freezes'' when the solid fraction increases above about $\nu=0.53$. The particles are packed too densely for them to change positions easily, and each particle is trapped in a ''cage'' of its neighbors. A whole assembly of densely packed particles can move as a unit, but if it any region is to shear, the density must be locally lowered there. Thus in the densest simulations in Fig. 17, a shear wave, which is essentially a parallel flow, is inhibited. Instead we find that the system finds another coherent motion where two counter-rotating, quasihexagonal eddies share the domain (see Fig. 18). We have not attempted to quantify this hexagonal state, though it is clearly distinct from the kinetic-sheared dichotomy described earlier.

V. DISCUSSION AND CONCLUSION

In this paper we have discussed the simplest example of a granular medium in the kinetic regime. Earlier works have demonstrated that this cooling inelastic gas is unstable to inhomogeneous fluctuations. Here our main focus has been to describe the various evolutionary paths which are followed once these fluctuations grow to finite amplitude and to delineate the regime boundaries in the three-dimensional parameter space (N,r,ν).

Provided that the medium is not too dense (i.e., $\nu\leqslant 0.7$) we believe that the major distinction is between simulations which evolve into the shearing state described by Goldhirsch and Zanetti [5] and those which collapse, as described by

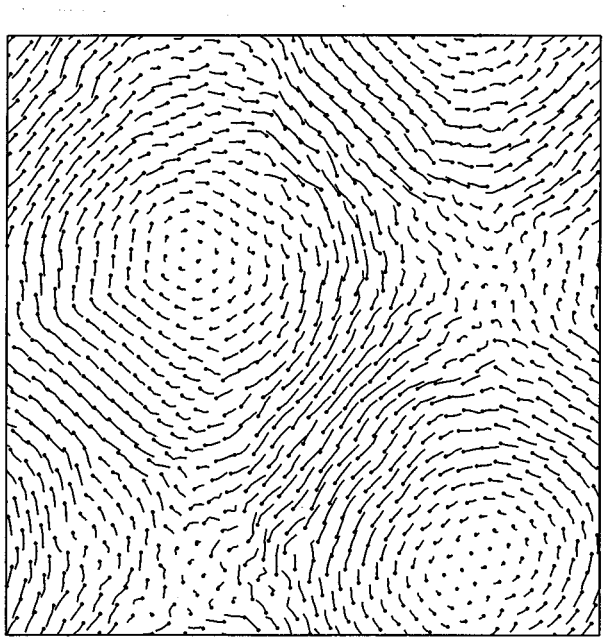

FIG. 18. Quasihexagonal eddies in a simulation with $\nu=0.8$ and $N=1024$.

McNamara and Young [8]. We have also described a clustering state which is observed as a long-lived transient: some simulations in the clustering state eventually evolve into the shearing state, while others collapse. In simulations of densely packed disks (i.e., $\nu \geqslant 0.7$) we saw a third possibility, namely, the quasihexagonal eddying state in Fig. 18. We have not attempted a detailed investigation of this tertium quid.

Our computational study has made contact with theory at two points. First, as shown in Fig. 14, the critical coefficient of restitution for an inelastic collapse is approximately predicted by the theories of the one-dimensional inelastic collapse constructed by Bernu and Mazighi [7] and McNamara and Young [2]. In retrospect, this agreement is not too surprising because the collapse event, once it begins, is almost one dimensional and is localized in space. Thus at the time of singularity, both the two-dimensional dynamics of the medium, and the total number of particles in the medium, are irrelevant. But it is surprising that the number of particles in these ''collapse strings'' is roughly equal to the number of particles in an optical depth, i.e., the number is roughly equal to $\lambda/d \sim \sqrt{N\nu}$. Since the collapse strings are formed when a group of particles are rattling around in a cluster, the success of the ''optical depth scaling'' shows that the cluster formation process detects the length of the domain. To amplify this point: if all the particles were simply swept together into a roughly circular cluster in the middle of the domain then collapse would depend only upon N and not on ν. But instead we find that collapse depends on the combination $\sqrt{N\nu}$—this is the content of Figs. 13 and 14.

The second point of contact between our computational study and theory is the success of Eq. (12) when $\nu \leqslant 0.7$ in predicting the critical value of the coefficient of restitution at which the shear mode first becomes unstable as r is decreased from the elastic limit $r=1$. This comparison between simulation and theory is contained in Figs. 16 and 17.

ACKNOWLEDGMENTS

This research was supported by ONR-N00014-92-J-1446. This work was improved by discussions with Brad Werner. We thank Rick Salmon for drawing our attention to Ref. [10]. We also thank Lisa Lehmann for her help with the figures.

[1] P. K. Haff, J. Fluid Mech. **134**, 401 (1983).
[2] S. McNamara and W. R. Young, Phys. Fluids A **4**, 496 (1992).
[3] S. McNamara and W. R. Young, Phys. Fluids A **5**, 34 (1993).
[4] N. Sela and I. Goldhirsch, Phys. Fluids **7**, 507 (1995).
[5] I. Goldhirsch and G. Zanetti, Phys. Rev. Lett. **70**, 1610 (1993).
[6] I. Goldhirsch, M. L. Tan, and G. Zanetti, J. Sci. Comp. **8**, (1993).
[7] B. Bernu and R. Mazighi, J. Phys. A **23**, 5745 (1990).
[8] P. Constantin, E. Grossman, and M. Mungan, Physica D **83**, 409 (1995).
[9] S. McNamara and W. R. Young, Phys. Rev. E **50**, R28 (1994).
[10] C. Eckart (unpublished).
[11] D. C. Rapaport, Comput. Phys. Rep. **9**, 1 (1988).
[12] M. P. Allen and D. J. Tildesley, *Computer Simulations of Liquids* (Oxford University Press, New York, 1987).
[13] P. K. Haff, in *Granular Matter*, edited by A. Mehta (Springer-Verlag, Berlin, 1994).
[14] S. Luding, E. Clement, A. Blumen, J. Rajchenbach, and J. Duran, Phys. Rev. E **50**, 4113 (1994).
[15] S. Luding, E. Clement, A. Blumen, J. Rajchenbach, and J. Duran, Phys. Rev. E **49**, 1634 (1994).
[16] J. T. Jenkins and M. W. Richman, J. Fluid Mech. **192**, 313 (1988).
[17] J. T. Jenkins and M. W. Richman, Phys. Fluids **28**, 3485 (1985).
[18] S. McNamara, Phys. Fluids A **5**, 3056 (1993).
[19] J. T. Jenkins and M. W. Richman, Arch. Ration. Mech. Anal. **87**, 355 (1985).
[20] Y. Limon Duparcmeur, H. Hermann, and J. P. Troadec, J. Phys. (France) I **5**, 1119 (1995).
[21] J. T. Jenkins and M. Shahinpoor, in *Mechanics of Granular Materials: New Models and Constitutive Relations*, edited by J. T. Jenkins and M. Satake (Elsevier, Amsterdam, 1983).